Electronic phase diagram of high temperature copper oxide superconductors

U. Chatterjee[1,2], D. Ai[1,2], J. Zhao[1,2], S. Rosenkranz[2], A. Kaminski[3], H. Raffy[4], Z. Z. Li[4], K. Kadowaki[5], M. Randeria[6], M.R. Norman[2] & J. C. Campuzano[*1,2]

[1]*Department of Physics, University of Illinois at Chicago, Chicago, IL 60607*

[2]*Materials Science Division, Argonne National Laboratory, Argonne, IL 60439*

[3]*Ames Laboratory and Department of Physics and Astronomy, Iowa State University, Ames, IA 50011*

[4]*Laboratorie de Physique des Solides, Universite Paris-Sud, 91405 Orsay Cedex, France*

[5]*Institute of Materials Science, University of Tsukuba, Ibaraki 305, Japan*

[6]*Department of Physics, The Ohio State University, Columbus, OH 43210*

[*]To whom correspondence should be addressed; E-mail: jcc@uic.edu.

$Bi_2Sr_2CaCu_2O_{8+\delta}$ Samples

The range of sample doping values together with their T^* and T_{coh} used in this work is shown in Table 1. The crystals were grown in traveling solvent floating zone furnaces, and the thin films were grown using an RF sputtering process. For all the samples, both films and single crystals, $T_c^{max} = 91$K. All samples were characterized by x-ray diffraction, and their T_c's determined by where the resistance $R(T)$ becomes zero within the uncertainty of the measurement. The samples were doped by changing their oxygen content through an annealing process. The doping value was determined from the Presland *et al*. formula[1] $T_c/T_c^{\max} = 1 - 82.6(\delta - 0.16)^2$.

T_c	δ (holes/Cu)	T^*	T_{coh}
UD55K	0.091	230	55
UD70K	0.107	220	70
UD85K	0.132	185	85
UD89K	0.144	156	89
OPT91K	0.160	135	115
OD87K	0.183	110	
OD83K	0.193		
OD80K	0.198	95	200
OD67K	0.216	67	231
OD65K	0.219	65	
OD60K	0.224	60	250
OD58K	0.226	58	270
OD55K	0.229	55	

Table 1: T_c (in K), doping (δ), T^*, and T_{coh} for the samples used in this work.

ARPES measurements

ARPES measurements were carried out at the Synchrotron Radiation Center, Wisconsin, and the Swiss Light Source, using Scienta R2002 and R4000 analyzers. 22 eV photons with polarization parallel to (0, 0)–(π, 0) were used, in order to maximize the signal at the antinode. The energy resolution was 15 - 20 meV (FWHM) with a k-

resolution between 0.01 and 0.0055 Å^{-1}. Raw energy distribution curves (EDCs) as a function of T for four representative doping values are shown in Fig. S1. In order to eliminate the temperature effects of the Fermi function, we divide the photoemission data by a resolution broadened Fermi function and determine $\mathbf{k}_F$ from the spectrum which (a) has a peak at the chemical potential when the system is gapless, or (b) the peak is closest to the chemical potential when the system is gapped[2], both in the superconducting and pseudogap states.

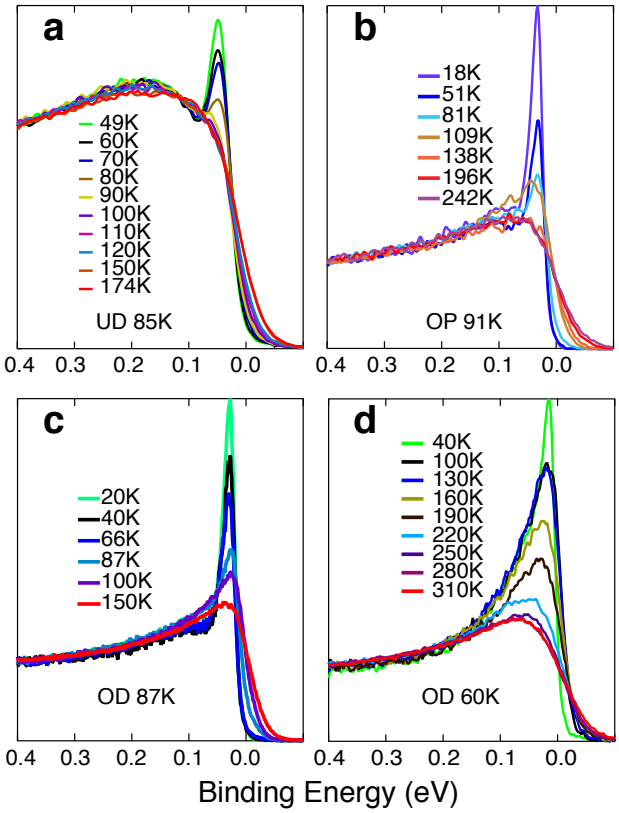

Figure S1 | Raw ARPES data vs. temperature and doping. | Raw EDCs at the antinode as a function of T for the data shown in the text. **a** an UD 85K sample; **b** an OP 91K sample; **c** an OD 87K sample, and **d** an OD 60K sample.

Choice of *k* point

In this work we focus on a single k-point, namely the antinode, because the spectra at this point show the most dramatic temperature and doping dependences (in other works we have extensively studied the k-dependencies as well). We first measure the entire Fermi surface, as shown in Fig. S2**a**.

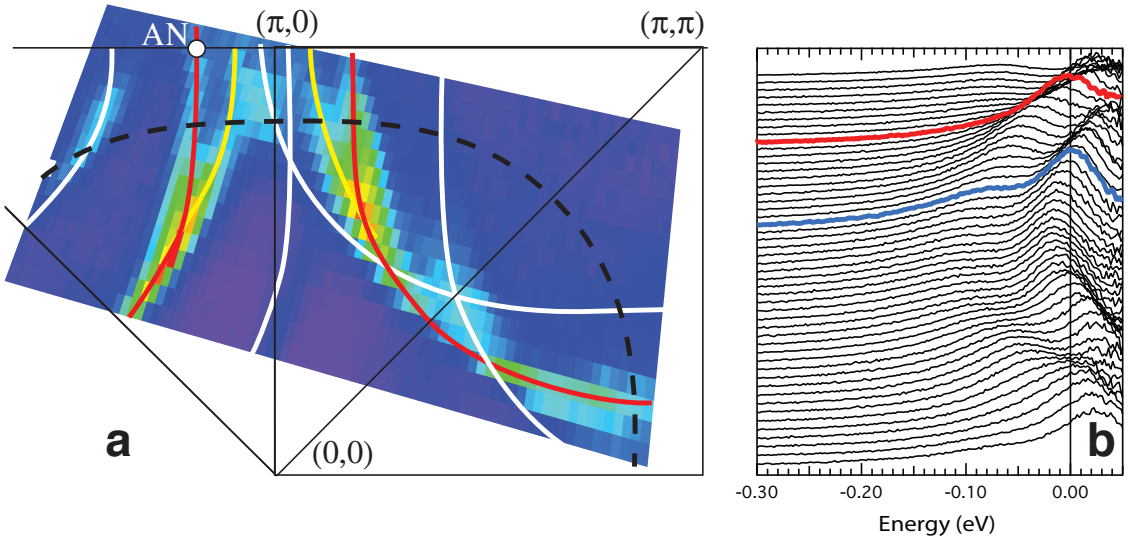

Figure S2 | **Choice of *k*-point. a** ARPES intensity at 28 meV binding energy as a function of k_x and k_y for a T_c = 87K sample at T = 40K, which exhibits bilayer splitting. The main bonding Fermi surfaces are indicated by red lines, the antibonding Fermi surfaces by yellow curves, and the replica superlattices that we observe by white lines. The dashed line indicates the position of the shadow Fermi surface, which is not observed in our experiments. The antinodal k_F of the bonding band where all the data in this work were obtained, is indicated by a white point labelled AN. It can be seen that at this point, there is no interference from the replica bands. **b** Illustration of the difference between taking data for an overdoped 55K sample (T = 100K) at the antinode of the antibonding band (blue curve), where the bilayer splitting can be seen, and at the antinode of the bonding band (red curve), where only one peak is seen.

One can see from that figure that at the antinodal point for the bonding band, indicated by a white dot, there is no interference from other bands. This is also clearly visible in the EDCs shown in Fig. S2**b**. We choose 22 eV because the cross section for both bonding and antibonding bands is high, as shown in Fig. S2**a**. We choose the antinodal point of the bonding band in the Y-quadrant because a) the gap is maximal there; b) coherence is easily defined there; c) the main and shadow bands do not intersect one another, and d) there is no interference from the replica superlattice bands either. We pick the bonding band because at its antinode, we miss the superlattice and shadow bands, as shown in Figs S3. Under the experimental conditions used in this work, we do not observe higher order replicas.

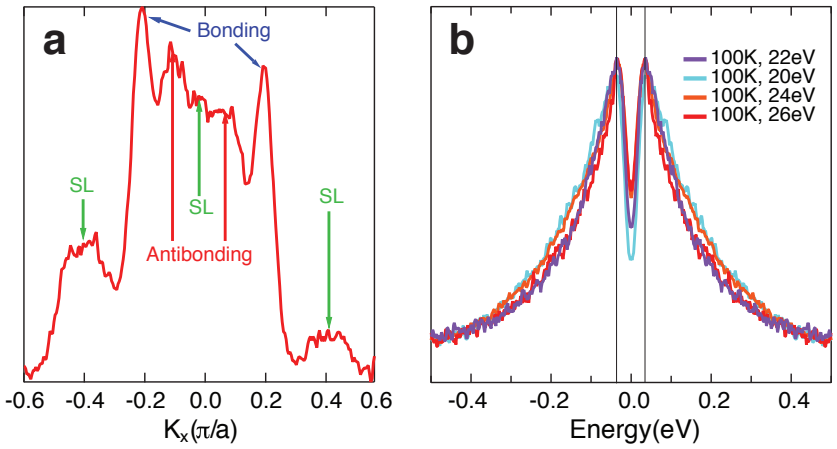

Figure S3 | **Bilayer splitting and photon energy dependence. a** MDC of an optimally doped sample at T = 20K and binding energy of 26 meV, showing clear signature of bilayer split band. Momentum cut is along the (π,0) -> (π,π) direction. The superlattice replicas are labelled SL. **b** EDCs of an optimally doped sample at 100K at the antinode for the bonding band (where the antibonding band is unoccupied), after background subtraction[3] and normalization. It can be seen that there are no changes in the spectral function lineshape once the background and normalization have been taken into account.

Photon energy dependence

The ARPES matrix element has a strong photon energy dependence[3], which might obscure additional peaks in the spectra, leading to an incorrect conclusion. On the other hand, spectra used in this work were obtained at a single photon energy. However, our measurements are at the Fermi momentum of the bonding band, by which point the antibonding band has dispersed above E_F, so it does not alter the spectra used in this work. In Fig. S4**b** we show the photon energy dependence of the bonding band at the antinodal point for an optimally doped sample at 100K. After subtracting the background[3] and normalizing the intensities to high binding energies (500 meV below the chemical potential), the matrix element effects have effectively been removed from the spectra, resulting in spectral shapes that are essentially independent of photon energy. We use an "unoccupied" state spectrum at a k far above k_F as an energy-dependent background.

Spectral signatures of T_{coh}

We find that we can model the broad, incoherent part of the spectrum with a lorentzian centered at E_F, and the sharp, coherent piece with a gaussian (a similar decomposition has been used in the very different context of the analysis of critical scattering[4]). The spectra clearly exhibit the same lineshape for all δ and T beyond 200 meV, corresponding to a lorentizan at E_F. Two adjustable parameters remain, namely the width and height of the gaussian component. A fit is shown in Fig. S4**a**. The same procedure works equally well when a spectral gap is present, by simply shifting the gaussian peak position from E_F to the measured gap energy, with no other adjustments, as illustrated in Fig. S4**b**.

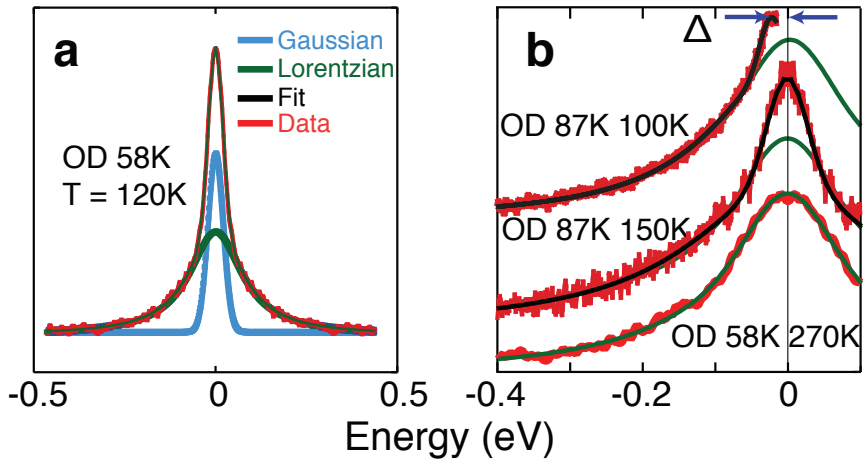

Figure S4 | Functional form of the spectra. **a** Fits (black curve) of the symmetrised antinodal spectrum (red curve) to a narrow gaussian (blue curve) and a broad lorentzian (green curve) for a sample with $\delta = 0.226$, taken at $T = 120$K. **b** Comparison of symmetrised spectra (red curves) with a gap (upper curve) and without a gap (lower curves). Black curves are the same fits as described in **a**, with the green curves representing the broad lorentzian peak.

In addition to identifying the sharp peak via a decomposition of the spectrum into a broad lorentzian and a sharp gaussian, the presence of a sharp peak can also be deduced directly from the raw spectra. A sharp break in the slope of the raw spectra is present at the binding energy where the coherent region of the spectra merges into the incoherent part, as shown in Fig. S5**a**. For $T > T_{coh}$, no break is discernible. For spectra with sufficiently high signal-to-noise ratio, the break can also be identified from the sudden increase in the derivative of the spectra, as shown in Fig. S5**b**. In Fig. S5**c** we demonstrate that for temperatures below T_{coh}, the spectra cannot be fitted by a single lorentzian (red curve). Additionally, we point out that the break occurs where the spectra deviates from the lorentzian component (light blue curve) of the full fit (purple curve).

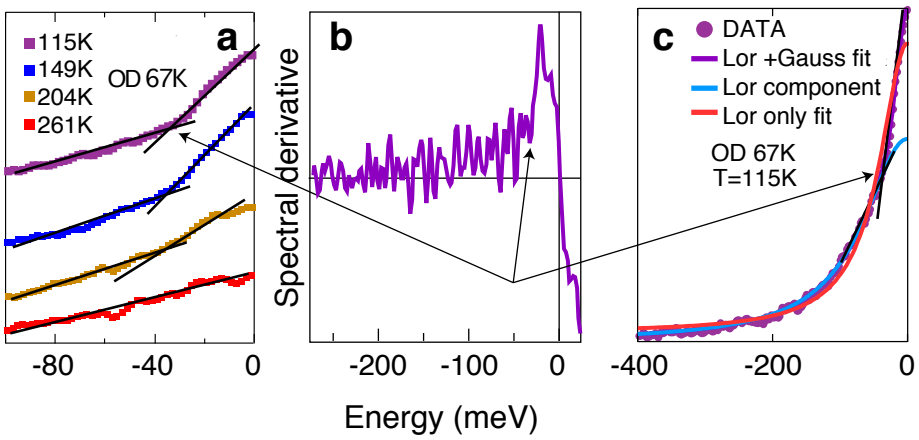

Figure S5 | Additional signatures of spectral coherence. **a** Spectra for an OD 67K sample for a small range of binding energies, at different temperatures. The top three spectra show a break where the coherent component merges with the incoherent one. The straight lines are guides to the eye. **b** Derivative of the top spectrum shown in **a**. The sharp change in the slope at the break point is indicated by the arrows. **c** Plot showing that a single lorentzian (red line) cannot fit the data (purple dots). The lorentzian component of the Gaussian plus lorentzian fit (purple curve) is shown as a light blue line. The two black lines are guides to where the slope in the spectra changes where the data deviate from the lorentzian component of the full fit.

The loss of coherence at higher temperatures is a generic phenomenon in cuprates. We demonstrate this in Fig. S6, where we show the temperature dependence of the spectra at the antinode for a single layer Bi2201 sample, with a $T_c \sim 0$K. As this sample is very overdoped, its T_{coh} is very high (if it indeed exists) and we therefore do not see the complete disappearance of the sharp peak. However, the results are qualitatively similar to those from Bi2212, namely the peak intensity decreases with increasing temperature.

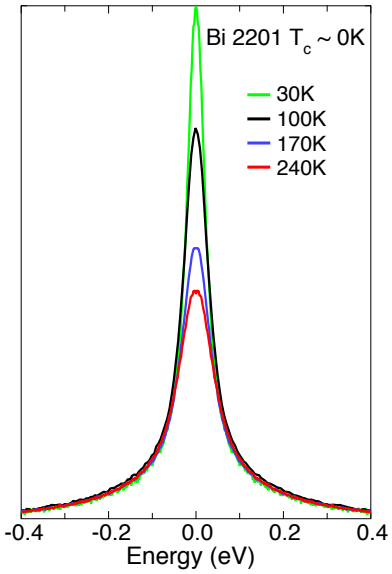

Figure S6 | Symmetrized spectra for a single-layer cuprate at the antinode as a function of temperature. As the temperature increases the spectrum loses intensity, mostly due to a loss of the coherent part. This sample is extremely overdoped, therefore we cannot reach its T_{coh} (if indeed it has one).

Sample aging

Since the data presented here are obtained at high temperatures, it is important to ensure that the samples do not age. By aging we mean that the doping of the sample changes during the measurement process. The linear variation of the superconducting or pseudogap with doping[5] allows us to monitor the change in doping of the sample. In Fig. S7**a** we show a sample becoming more underdoped. In Fig. S7**b** a sample becomes more overdoped. In Fig. S7**c** we show the case where a sample does not age. Upon increasing the temperature from 83K to 100K, and subsequently lowering it to 40K, the value of the gap remains unchanged.

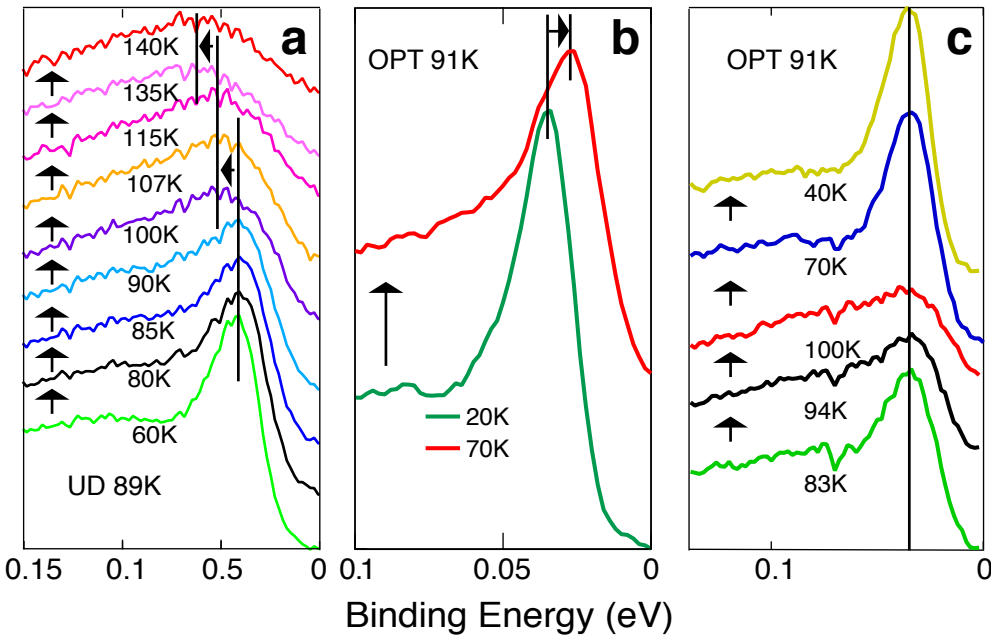

Figure S7 | **Effects of sample aging for different samples.** EDCs at the antinode. **a** an underdoped sample becoming more underdoped at elevated temperatures. The temperature increases sequentially from the bottom to the top spectra, as indicated by the arrows. **b** Sample becoming more overdoped with increasing temperature. **c** Sample doping remains constant as the temperature changes. Data were obtained sequentially from the bottom curve at 83K, increased to 100K, and subsequently reduced to 40K, with no change in the gap value.

References

1. Presland MR, et al. (1991) General trends in oxygen stoichiometry effects on T_c in Bi and Tl superconductors. *Physica* C 176:95-105.

2. Kanigel A, et al. (2006) Evolution of the pseudogap from Fermi arcs to the nodal liquid, *Nature Phys.* 2:447-451.

3. Kaminski A, et al. (2004) Identifying the background signal in angle-resolved photoemission spectra of high temperature superconductors. *Phys. Rev.* B 69:212509.

4. Campuzano JC, et al. (1985) Au(110) (1x2)-to-(1x1) Phase Transition: A Physical Realization of the Two-Dimensional Ising Model. *Phys. Rev. Lett*. 54:2684-2687.

5. Campuzano JC, et al. (1999) Electronic spectra and their relation to the (π, π) collective mode in high-T_c superconductors. *Phys. Rev. Lett.* 83:3709-3712.